Chemical Engineering Journal 442 (2022) 136129

Contents lists available at ScienceDirect

Chemical Engineering Journal

journal homepage: www.elsevier.com/locate/cej

A novel π-d conjugated cobalt tetraaza[14]annulene based atomically dispersed electrocatalyst for efficient CO_2 reduction

Zhifu Liang [a,c,1], Ting Zhang [a,c,1], Pengfei Cao [b,g,*], Takefumi Yoshida [d], Weiqiang Tang [e,*], Xiang Wang [c], Yong Zuo [c], Pengyi Tang [f], Marc Heggen [g], Rafal E. Dunin-Borkowski [g], Joan Ramon Morante [c], Andreu Cabot [c,j,*], Masahiro Yamashita [h,i], Jordi Arbiol [a,j,*]

[a] Catalan Institute of Nanoscience and Nanotechnology (ICN2), CSIC and BIST, Campus UAB, Bellaterra, 08193 Barcelona, Catalonia, Spain
[b] School of Chemical Engineering and Technology, Xi'an Jiaotong University, Xi'an 710049, China
[c] Catalonia Institute for Energy Research – IREC, Sant Adrià de Besòs, Barcelona 08930, Catalonia, Spain
[d] Innovation Research Center for Fuel Cells, The University of Electro-Communications, Chofu, Tokyo 182-8585, Japan
[e] State Key Laboratory of Chemical Engineering and School of Chemical Engineering, East China University of Science and Technology, Shanghai 200237, China
[f] State Key Laboratory of Information Functional Materials, 2020 X-Lab, ShangHai Institute of Microsystem and Information Technology, Chinese Academy of Sciences, Shanghai 200050, China
[g] Ernst Ruska-Centre for Microscopy and Spectroscopy with Electrons and Peter Grünberg Institute Forschungszentrum Jülich GmbH, 52425 Jülich, Germany
[h] Department of Chemistry, Graduate School of Science, Tohoku University, 6-3 Aramaki-Aza-Aoba, Aoba-Ku, Sendai 980-8578, Japan
[i] School of Materials Science and Engineering, Nankai University, Tianjin 300350, China
[j] ICREA, Pg. Lluís Companys 23, 08010 Barcelona, Catalonia, Spain

ARTICLE INFO

Keywords:
Tetraaza[14]annulene
π-d Conjugated
Atomically dispersed Co catalyst
Electrocatalytic CO_2 reduction

ABSTRACT

Tetraaza[14]annulenes (TAA) are synthetic macrocycles which are analogue to porphyrins. However, there are almost no reports about the synthesis of polymers based on TAA and neither on their use as electrocatalysts. The study of new catalysts to promote an efficient electrochemical conversion of carbon dioxide to valuable chemicals is a promising approach to relieve the pressure of carbon emissions and realize the carbon cycle. Herein, we first report the synthesis of a novel tetraaza[14]annulene (TAA) based organic polymeric metal complex (PMC) by a non-template method. This PMC is used as ligand to construct a π-d conjugated cobalt coordination polymer (Poly-TAA-Co) with CoN_4 structure which is supported on multi-wall carbon nanotubes (CNTs) to work as an atomically dispersed efficient electrocatalyst for the CO_2 reduction reaction (CO_2RR). The resulting catalyst (Poly-TAA-Co-CNT) exhibits excellent performance, with a 90% CO faradaic efficiency, a low overpotential (390 mV) and good stability in 0.5 M $KHCO_3$ aqueous solution. Density functional theory calculations confirmed that the cobalt tetra[14]annulene is an excellent active site for electrocatalytic CO_2RR. This work not only inspires the design of novel TAA based macromolecules, but also paves the way to the development and application of new molecular-based catalysts for electrocatalytic CO_2RR.

1. Introduction

Tetraaza[14]annulenes (TAA) are a type of synthetic macrocycles analogue to porphyrins, which have been much less studied [1–4]. They contain four nitrogen atoms in a central cavity that can be easily deprotonated and coordinated with metal ions to form tetra[14]anulene metal coordination structures. Metal complexes based on TAA have been used in field-effect transistors [5], CO electrochemical oxidation [31], as single molecular magnets [6], catalysts [7] and dye-sensitized solar cells [8]. Most of the previous studies used the metal ion as a template for the synthesis of the TAA complexes. However, this type of macrocycles have been rarely used to build polymeric metal complexes (PMCs), because

* Corresponding authors at: Catalan Institute of Nanoscience and Nanotechnology (ICN2), CSIC and BIST, Campus UAB, Bellaterra, 08193 Barcelona, Catalonia, Spain (J. Arbiol); State Key Laboratory of Chemical Engineering and School of Chemical Engineering, East China University of Science and Technology, Shanghai 200237, China (W. Tang); Catalonia Institute for Energy Research - IREC, Sant Adrià de Besòs, Barcelona 08930, Catalonia, Spain (A. Cabot); School of Chemical Engineering and Technology, Xi'an Jiaotong University, Xi'an 710049, China (P. Cao).
E-mail addresses: p.cao@fz-juelich.de (P. Cao), wqtang@ecust.edu.cn (W. Tang), acabot@irec.cat (A. Cabot), arbiol@icrea.cat (J. Arbiol).
[1] These authors Zhifu Liang and Ting Zhang contributed equally to this work.

https://doi.org/10.1016/j.cej.2022.136129
Received 18 January 2022; Received in revised form 27 March 2022; Accepted 28 March 2022
Available online 29 March 2022

the suitable organic precursors are too little to work as linkage ligand between metal atoms. In addition, most of the tetraaza[14]annulene complexes use the template synthesis method, namely, the metal ion is working as template which makes it more difficult and limited to be developed. Recently, Y. Jiang and co-workers reported the first two-dimensional (2D) Ni(II)-based TAA-linked metal organic frameworks (MOFs) by a template method, and characterized its electrical conductivity and magnetic properties [9]. We believe that these novel structures are excellent platforms for electrocatalytic applications, but a more in-depth exploration of these novel TAA-based PMCs with atomically dispersed metal atoms and the study of their relative catalytic performance are needed.

The utilization of renewable energy to drive the electrocatalytic reduction of carbon dioxide to valuable chemicals is a potentially cost-effective strategy to promote the carbon cycle. In this direction, the search for electrocatalysts [10,67] and photocatalysts [63] able to efficiently activate the CO_2 reduction reaction (CO_2RR) and explore other green energy sources [64] have attracted a strong interest during the past years. Most electrocatalytic materials reported for CO_2RR are nanomaterials [11,12,39–41,45,46,52,53]. Even though these nanomaterials have displayed efficient catalytic activity toward electrochemical CO_2 reduction, [42] most are not easy to be synthesized in large quantities while controlling the active sites under a mild and easy controllable condition and the metal atoms are not 100% utilized. Recently, atomically-dispersed metal-based catalysts, especially those with a coordination structure of metal-N_4, have been successfully applied to high-efficiency electrocatalytic carbon dioxide reduction due to their high catalytic activity and 100% atom utilization [32,43]. However, due to that most are prepared from the general high-temperature pyrolysis method, the active site structure and the ligand structure are not easy to be determined and controlled [10,24]. In contrast, molecular catalysts also work as a type of atom dispersed catalysts, which can be easily prepared under mild and controllable conditions and provide a well-defined platform that facilitates the understanding of the structure-performance relationships, thus enabling a rational catalyst design and optimization. Combining the merits of these two worlds, the development of stable and high-performance heterogeneous molecular catalysts is raising increasing interest [13,14].

In recent years, molecular catalysts based on metalloporphyrin and metallophthalocyanine supported on multi-wall carbon nanotubes (CNTs) have shown low overpotentials, high Faradaic efficiencies and excellent selectivity for electrocatalytic CO_2RR [15–19]. However, small molecular catalysts are not easily to work for heterogeneous reduction reactions, which limits their application [20,21]. Therefore, it is challenging to develop novel materials and molecular engineering strategies to realize the highly efficient and stable molecular electrocatalysts that an efficient CO_2RR would require. Alternatively, π-d conjugated PMCs, with a hybrid interaction between the π orbital of the ligand with the d orbital of the transition metal, have aroused widespread interest in recent years [34–38]. This hybrid interaction is similar to that presented in the π-π conjugated organic polymer, with the advantages such as their functionalization flexibility through ligand engineering design. However, the π-d conjugated PMCs have been less studied for electrocatalytic CO_2 reduction. In the present work we combine the π-d conjugated structure and the Tetraaza[14]annulenes macrocyclic structure to design a novel atomically dispersed cobalt atom catalyst as efficient electrocatalysts for CO_2 reduction.

Herein, a non-template synthesis method was used to construct a new type of Tetra[14]annulene based π-d conjugated metal organic polymer, namely, Poly-TAA-Co with CoN_4 structure. This macromolecular complex is loaded on a conductive support, namely multi-wall CNTs, and applied for the efficient electrochemical CO_2RR. The obtained results have been rationalized by means of density functional theory (DFT) calculations.

2. Experimental section

2.1. Materials

Methanol (99%), N,N-dimethylformamide (DMF) (98%), hydrazine hydrate (98%) and carbon paper were purchased from Alfa Aesar. 1,2,4,5-benzenetetraamine tetrahydrochloride, potassium thiocyanate (99%), and Nafion (10%) were purchased from Sigma-Aldrich. Cobalt acetate tetrahydrate (99%), potassium hydrogen carbonate (99.7%), 1-butanol (99%), and 2-(4-pyridyl)malondialdehyde (95%) were bought from Acros Organics. All solutions were prepared with Milli-Q water (DI-H_2O, Ricca Chemical, ASTM Type I). Nafion membreanes (N-117 membrane, 0.18 mm thick) was purchased from Alfa Aesar and kept in 0.5 M NaOH solution. All chemicals were used without further purification. Carbon Nanotubes (CNTs) was ordered from Sailed Technology.

2.2. Synthesis of Poly-TAA

2-(4-Pyridyl)malondialdehyde (149 mg, 1 mmol), 1,2,4,5-benzenetetraamine tetrahydrochloride (142 mg, 0.5 mmol) and 6 mL 1-butanol were added to a 25 mL three-neck round bottom flask. Then a few drops of acetic acid were added. The resulting solution was sonicated for half an hour to obtain a homogenous mixture. The mixture was heated to 110 °C with stirring under argon for 48 h and afterward cooled to room temperature. The resulting brown precipitate was collected by vacuum filtration and washed with ethanol, then Soxhlet extracted with methanol for 24 h, then vacuum dried at 60 °C for 24 h to give a brown powder with ~ 63% yield.

2.3. Synthesis of Poly-TAA-Co

Poly-TAA (60 mg), cobalt(II) chloride hexahydrate (60 mg) and 6 mL DMF were added to a 15 mL three-neck round bottom flask. The resulting mixture was maintained at 130 °C with stirring under argon for 48 h and then cooled to room temperature. The resulting brown precipitate was collected by vacuum filtration and washed with ethanol, then vacuum dried at 60 °C for 24 h to give a brown-black powder with ~ 56% yield.

2.4. Synthesis of Poly-TAA-Co/CNT composites

The obtained Poly-TAA-Co and pre-oxidized carbon nanotubes (CNTs) were put into a 15 mL glass vial. Then 3 mL DMF were added. The resulting solution was sonicated for half an hour, then stirred at 100 °C for 12 h. The obtained black composites were filtrated and washed with ethanol, then vacuum dried at 60 °C for 24 h to get the composite.

2.5. Electrochemical measurements

5 mg of the Poly-TAA-Co-CNT and 100 μL 5 wt% Nafion solutions were dissolved in ethanol (1 mL) and ultrasonicated for 30 min to form an evenly suspension for the electrochemical experiments. To prepare the working electrode, 400 μL above as-prepared inks were dropped onto the two sides of the carbon paper electrode with 1×1 cm^2 and then dried at room temperature for a few minutes, resulting in a catalyst loading mass of ~ 2 mg/cm^2.

The electrocatalytic performance of different catalysts were measured at room temperature by using a gas-tight H-cell with two compartments separated by a cation exchange membrane (Nafion N-117 membrane) with a continuously Ar or CO_2 gas injection. Each compartment contained 70 mL electrolyte (0.5 M $KHCO_3$ made from deionized water). In a typical experiment, a standard three-electrode setup in 0.5 M $KHCO_3$ solution was assembled: an Ag/AgCl electrode as reference electrode, a Pt wire as auxiliary electrode and a carbon paper coated with the different samples as working electrode (surface area = 1

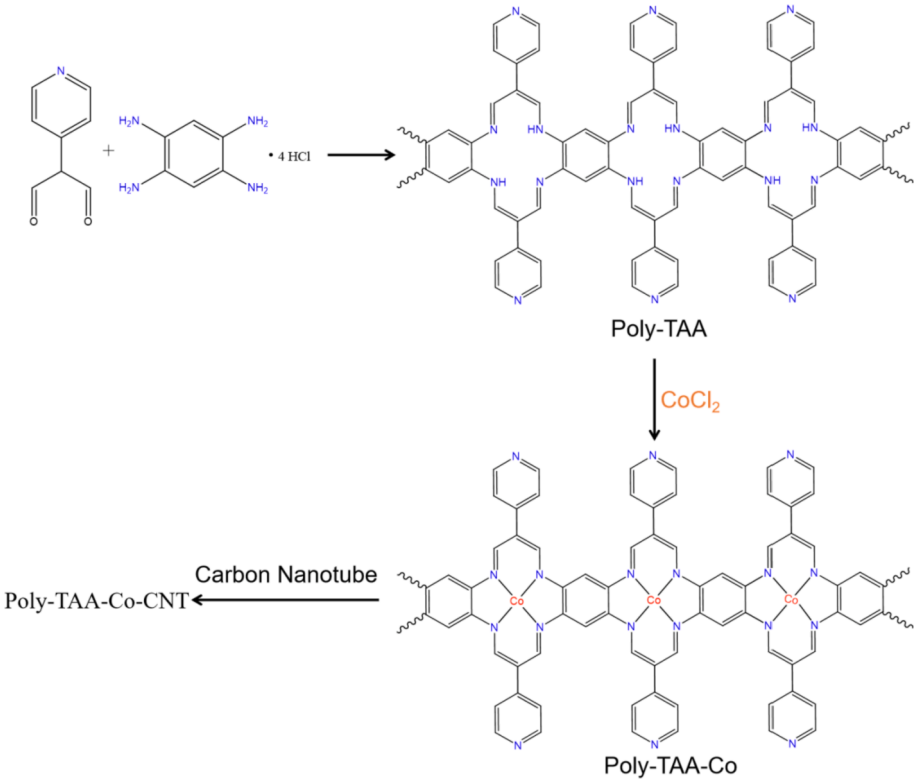

Scheme 1. Scheme of the synthesis of Poly-TAA-Co.

cm^2). The potentials were measured versus Ag/AgCl and converted to the reversible hydrogen electrode (RHE) according to the following equation: $E_{RHE} = E^0_{Ag/AgCl} + E_{Ag/AgCl} + 0.059 \times pH$, pH = 7 [44] All electrochemical results were recorded without iR-compensation by using a computer-controlled BioLogic VMP3 electrochemical workstation. Meanwhile, the *I-t* curves were obtained to reach a stable state at −0.30 V vs. RHE in Ar-saturated 0.5 M $KHCO_3$ (pH = 8.5) as supporting electrolyte. The CV and LSV curves were performed at 20 mV s^{-1}. Moreover, electrochemical impedance spectroscopy (EIS) of different samples were carried out in a frequency range from 100 kHz to 100 mHz.

Before the electrochemical CO_2 reduction experiments, an average rate of 20 mL min^{-1} Ar was injected into cathodic electrolyte in order to form an Ar-saturated solution. During the electrochemical CO_2 reduction experiments, the CO_2 gas was delivered at an average rate of 20 mL min^{-1} at room temperature and ambient pressure, and we measured the downstream by a volumetric digital flowmeter. The gas-phase composition was analyzed by gas chromatography (GC) during potentiostatic measurements every 20 min.

Details concerning the calculation of Faradaic Efficiency (FE) are shown below.[47,48].

The partial current density for a given gas product was calculated as below:

$$j_i = x_i \times V \times \frac{n_i F P_0}{RT} \times (electrode\ area)^{-1} \quad (1)$$

where x_i is the volume fraction of certain product determined by online GC referenced to calibration curves from three standard gas samples, v is the flow rate, n_i is the number of electrons involved, $P_0 = 101.3$ kPa, F is the Faraday constant, and R is the gas constant. The corresponding FE at each potential is calculated by.

$$FE = \frac{j_i}{j} \times 100\% \quad (2)$$

2.6. Characterizations

The crystal structure information was characterized by means of powder X-ray diffraction (XRD) measured in a Bruker AXS D8 Advance X-ray diffractometer. (Cu-Kα radiation, λ = 1.5106 Å, 40 kV and 40 mA; Bruker, Germany). High-resolution transmission electron microscopy (HRTEM) were conducted in a FEI Tecnai F20 microscope at an operating voltage of 200 keV equipped with an embedded Quantum Gatan Image Filter for electron energy loss spectroscopy (EELS) analyses. High angle annular dark-field (HAADF)-scanning transmission electron microscopy (STEM) images and Energy Dispersive X-Ray Spectroscopy (STEM-EDS) analysis were obtained in a spherical aberration corrected transmission electron microscopy FEI Titan G2 80–200 (ChemiSTEM). It is equiped with four EDX detectors and operated at 200 kV. High-resolution transmission electron microscopy (HRTEM) and high angle annular dark-field (HAADF)-scanning transmission electron microscopy (STEM) images were obtained in a FEI Tecnai F20 microscope at an operating voltage of 200 keV equipped with an embedded Quantum Gatan Image Filter for electron energy loss spectroscopy (EELS) analyses. Images had been analyzed by means of Gatan Digital Micrograph software. Thermogravimetric analyses (TGA) were performed under air at a heating rate of 5 °C/min using a Thermogravimetric Analyzer Q200. X-ray photoelectron spectroscopy (XPS) data was obtained by using 150 W and a Phoibos 150 MCD-9 detector. The X-ray absorption fine structure (XAFS) measurements of the pellet of powder sample were carried out at the BL12C beamline of the Photon Factory, the High Energy Accelerator Research Organization (KEK), under proposal no. 2019G117, 2021G129. Co foil was used for the calibration of Co K-edge. Structural analysis was performed using the Demeter software platform. The reported crystal data were used for calculating Feff. The samples were pressed onto a double-sided carbon tape and the data was recorded in the X-ray fluorescence mode. The XAFS data was processed with the ATHENA program.[49] The EXAFS was analyzed using the IFEFFIT package [50] and the EXAFS fitting was performed with FEFF6L.[51].

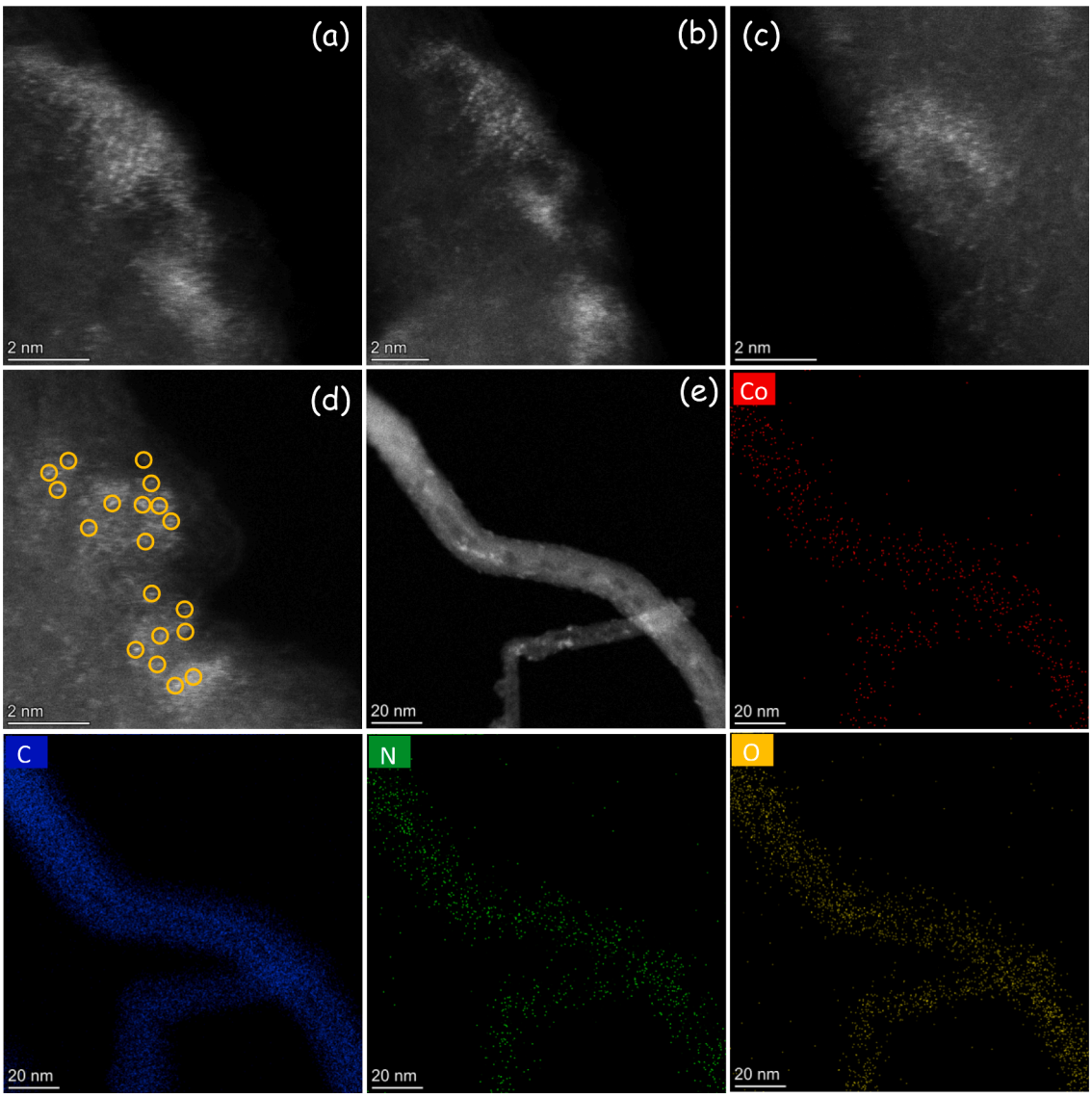

Fig. 1. (a)-(c) HAADF-STEM images of Poly-TAA-Co-CNT (3:7) displaying atomically dispersed cobalt atoms. (d) Low magnification HAADF-STEM image and EDS elemental maps for Co (red), C (light blue), N (green) and O (yellow).

2.7. DFT calculation details

The lowest unoccupied molecular orbital (LUMO) and highest occupied molecular orbital (HOMO) of cobalt phthalocyanine (CoPc) and Co(II) tetraaza[14]annulenes (CoTAA) structure unit were calculated by using DFT with the hybrid B3LYP functional and the 6–311++G (d,p) basis set.[57–59] For Co atoms the Stuttgart Dresden (SDD) triple zeta effective-core potential (ECP) basis set was used.[60] D3 dispersion correction developed by Grimme is included for weak interactions.[61] These calculations were carried out using the Gaussian16 program package.[62]. The visualization of the HOMO and LUMO plots is carried out using the Multiwfn 3.8 program and Visual Molecular Dynamics software [65,66].

The spin-polarized density functional theory (DFT) calculations with projector augmented wave (PAW) method were performed using the Vienna Ab initio Simulation Package code.[54,55] The generalized gradient approximation of Perdew-Burke-Ernzerhof (PBE) with van der Waals correlation was employed to optimize the geometric structures.[56] The convergence criteria was 0.03 eV/ Å in force and 1×10^{-5} eV in energy, while the plane wave cutoff was 500 eV. The Monkhorst–Pack mesh *k*-point grids was $4 \times 1 \times 1$ for all models. All the vacuum thicknesses were higher than 15 Å.

The whole process of CO_2 electrochemical reduction to CO mainly includes the following three steps:

$$CO_2(g) + * + H^+ + e^- \leftrightarrow COOH^* \text{ (Activation process)} \quad (1)$$

$$COOH^* + H^+ + e^- \leftrightarrow CO^* + H_2O(l) \text{ (Surface reaction)} \quad (2)$$

$$CO^* \leftrightarrow CO(g) + * \text{ (Desorption process)} \quad (3)$$

where the *, COOH* and CO* represent free sites, the adsorption state of COOH and CO, respectively. The (g) represent the gas phase. The reaction free energies of each steps were calculated by the following formula:

$$G = E_{DFT} + E_{ZPE} - TS + E_{sol} \quad (4)$$

where E_{DFT} is the DFT calculated energy, E_{ZPE} is the zero-point energy, T (=298.15 K) is temperture, S is the entropy, and E_{sol} is the solvation correction, which for CO* was stabilized by 0.1 eV and for COOH* by 0.25 eV.

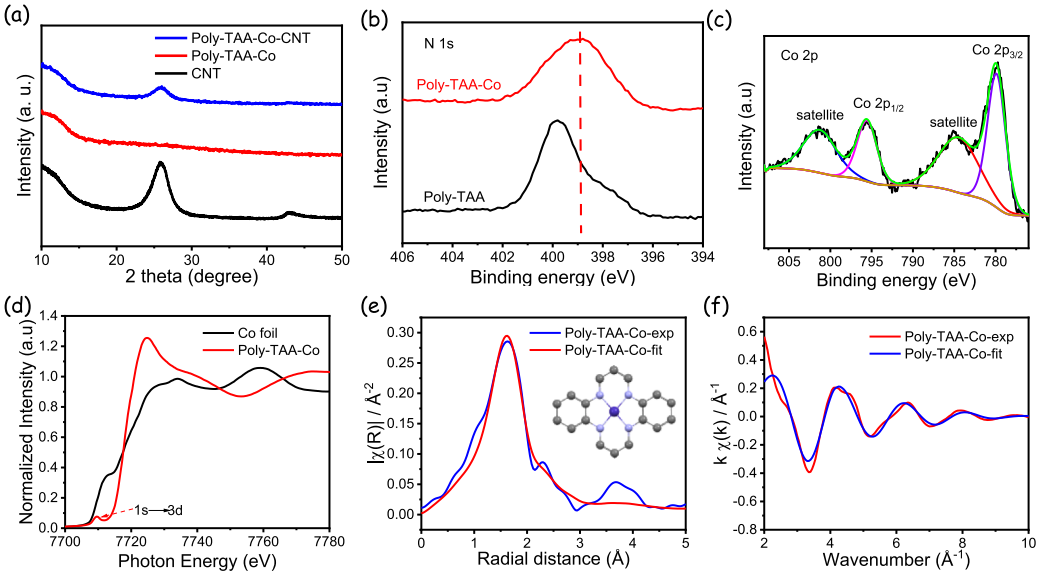

Fig. 2. (a) XRD patterns of CNT, Poly-TAA-Co and Poly-TAA-Co-CNT. (b) N 1 s and (c) Co 2p XPS spectra of Poly-TAA-Co powder. (d) Co K-edge XANES spectrum. (e) Fourier transformed EXAFS spectrum and fitted curve. (f) Co K-edge EXAFS oscillations in k-space (k3χ(k)) of Poly-TAA-Co and its fitted spectrum.

3. Results and discussions

3.1. Structural characterization

The Poly-TAA-Co conjugated polymer was prepared in two steps (Scheme 1). First, the Poly-TAA was synthesized by using a non-template method based on the Schiff base reaction between 2-(4-pyridyl)malondialdehyde and 1,2,4,5-benzenetetramine tetrahydrochloride in 1-butanol with a few drops of acetic acid. The obtained brown precipitate was Soxhlet extracted with methanol to remove the small impurity molecules and dried at 60 °C under vacuum. The brown color of the product was an indication of the formation of a conjugated organic polymer. In a second step, Poly-TAA was reacted with cobalt chloride in dimethylformamide (DMF) to yield metal organic polymer Poly-TAA-Co.

Fourier-transform infrared spectroscopy (FTIR) analysis of Poly-TAA-Co displayed the footprint of C═N at 1606 cm^{-1}, suggesting the formation of Co(II) tetraaza[14]annulene (**Figure S1**) [22]. The morphology of Poly-TAA-Co is displayed in **Figures S2 and S3**.

To improve the electrical conductivity of Poly-TAA-Co organic polymer toward their use as efficient electrocatalysts for CO_2RR, they were grafted through π-π interaction to the surface of pre-oxidized multi-wall CNTs by just mixing both in DMF (Scheme 1). Isolated Co atoms sites were characterized via high angle annular dark-field (HAADF)-aberration-corrected scanning transmission electron microscopy (STEM) analysis (Fig. 1**a-d**). The Energy Dispersive X-Ray Spectroscopy (EDS) analysis revealed the homogeneous distribution of Poly-TAA-Co on the surface of CNTs, and the uniform atomic distribution of Co within Poly-TAA-Co (Fig. 1**e**). The powder X-ray diffraction (PXRD) pattern of Poly-TAA-Co displayed no diffraction peak (Fig. 2**a**), which exposed the amorphous nature of the material and discarded the presence of any crystalline Co-based phase. The PXRD pattern of the obtained composite (Poly-TAA-Co-CNT) showed a unique peak at about 26°, which was assigned to the overlap between the CNT and the organic polymer structures.

X-ray photoelectron spectroscopy (XPS) analyses displayed the presence of C, N, O, Cl of Poly-TAA and Poly-TAA-Co (**Figure S4** and **Figure S5**). Compared with Poly-TAA, the high-resolution N 1 s XPS spectrum of Poly-TAA-Co is shifted to lower binding energies, which is attributed to the deprotonation of the nitrogen in the TAA cores upon coordination with cobalt ion (Fig. 2**b**) [9,30]. The high resolution Co 2p XPS spectrum of Poly-TAA-Co (Fig. 2**c**) showed two main peaks at 796 eV ($2p_{1/2}$) and 780.3 eV ($2p_{3/2}$), that are assigned to a Co^{2+} chemical state. The respective satellite peaks were also observed [29]. Thermogravimetric analyses (TGA) were performed under air to analyze the Cobalt content of Poly-TAA-Co (**Figure S6**). The small mass lost at about 100 °C corresponds to the solvent (mainly water). The poly-TAA-Co start to decompose at about 350 °C. Finally, after about 650 °C, Poly-TAA-Co fully decomposes to cobalt oxide. From the TGA analysis, we can calculate that the Co content of the Poly-TAA-Co is about 12.6% (the theoretical value was 14%). After loading the poly-TAA-Co on the CNTs, where the CNTs corresponding mass was 70%, the Co mass content in the Poly-TAA-Co-CNT (3:7) is 3.78%.

The coordination structure of cobalt in Poly-TAA-Co was further analyzed by means of X-ray absorption fine structure (XAFS) at the Co K-edge (Fig. 2**d-f**). The Co K-edge X-ray absorption near-edge structure (XANES) spectrum of Poly-TAA-Co exhibits the fingerprint of CoN_4 at 7709.4 eV assigned to the dipole forbidden 1s to 3d transition [16]. In addition, we observed the XANES absorption onset of Poly-TAA-Co at higher energy than that of cobalt foil (Fig. 2**d**). Besides, the main absorption peak of Poly-TAA-Co has a stronger intensity than that of Co foil. These features demonstrate the valence state of Co in Poly-TAA-Co to be higher than that of metallic cobalt, consistently with XPS results. The fitting of the Fourier transformed extended X-ray absorption fine structure (EXAFS) spectrum suggests that the Co is coordinated with 4 nitrogen atoms with a bond length of 2.05 Å (Fig. 2**e and Table S1**). Overall, XAFS analysis confirmed the formation of the CoN_4 structure units, thus demonstrating our synthetic route to yield Poly-TAA-Co (Scheme 1). The surface area of Poly-TAA, Poly-TAA-Co and Poly-TAA-Co-CNT, evaluated from N_2 adsorption–desorption isotherms at 77 K using the Brunauer-Emmett-Teller equation was 4.1, 124.9 and 208.2 $m^2\ g^{-1}$, respectively (**Figure S7**).

3.2. Electrochemical CO_2 reduction performance

The electrocatalytic activity toward CO_2RR of the Poly-TAA-Co metal organic polymer and it blended with two main different amounts of CNTs (Poly-TAA-Co:CNT = 3:7 and 1:1) were investigated using a three-electrode H-cell including an anion exchange membrane and a 0.5 M $KHCO_3$ electrolyte. Gas-phase products were periodically

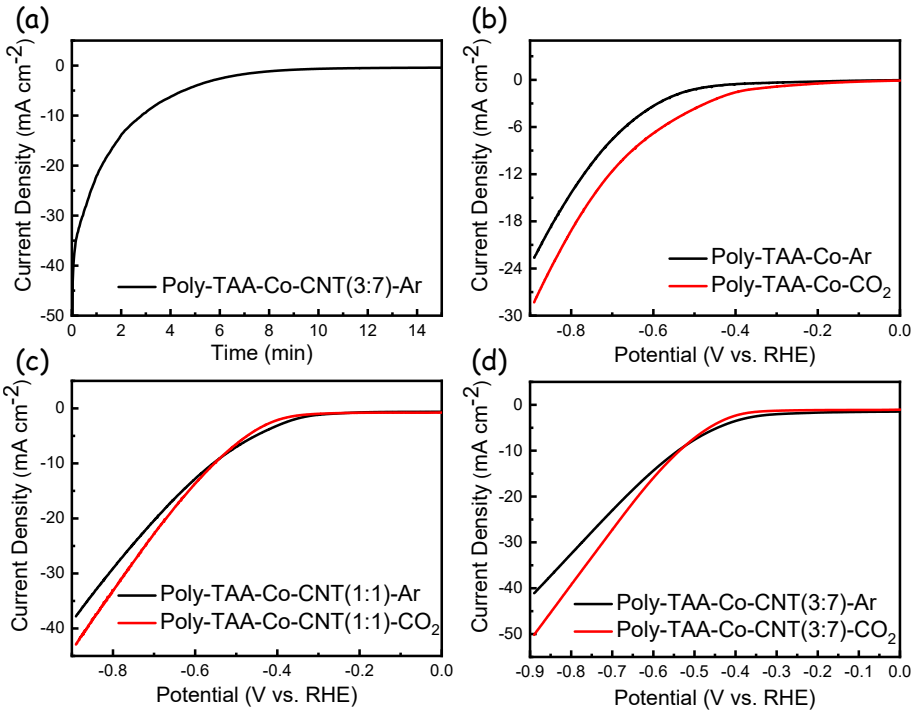

Fig. 3. (a) Electrode current recorded during reduction of Poly-TAA-Co-CNT(3:7) at −0.30 V vs. RHE in 0.5 M $KHCO_3$ purged with Ar gas. Linear sweep voltammetry (LSV) comparison for (b) Poly-TAA-Co, (c) Poly-TAA-Co-CNT(1:1) and (d) Poly-TAA-Co-CNT(3:7) samples in Ar- and CO_2-saturated 0.5 M $KHCO_3$ solution.

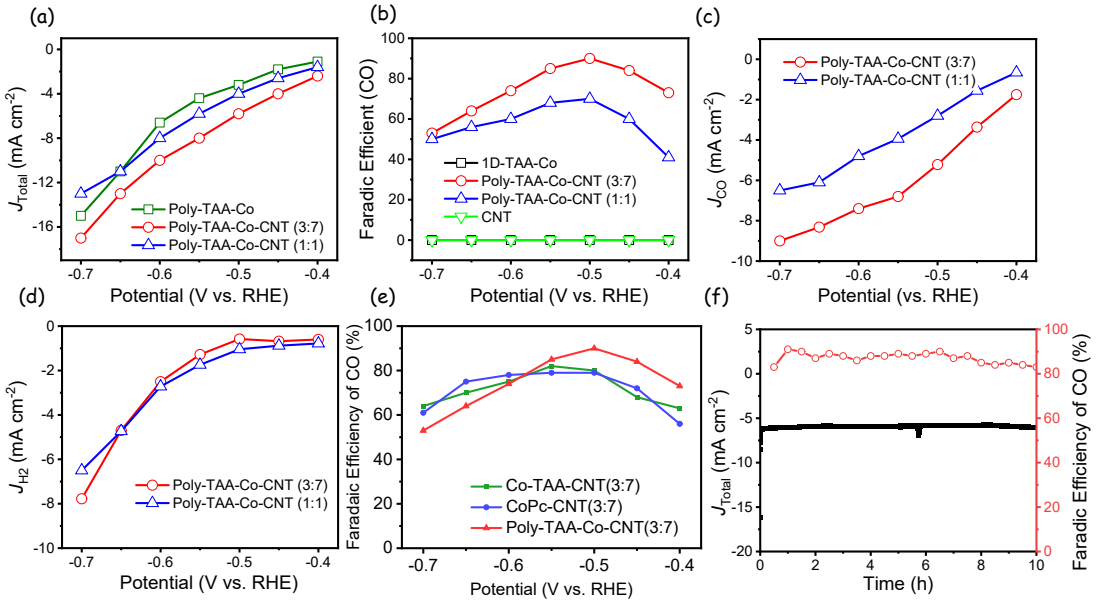

Fig. 4. (a) Total current density, (b) FE of CO at various potentials, (c) current density for CO production, (d) FE of H_2 at various potentials, (e) FE of CO at various potentials on Co-TAA-CNT(3:7), CoPc-CNT(3:7) and Poly-TAA-Co-CNT(3:7). (f) Stability test of Poly-TAA-Co-CNT(3:7) at −0.50 V vs. RHE.

quantified using gas chromatography (GC). Online GC results showed CO and H_2 to be the main gas products for all catalysts. Electrodes were prepared by coating the catalysts on carbon paper (1 cm × 1 cm) with a mass loading of ~ 2.0 mg cm^{-2}. Electrodes were pretreated at a constant potential of −0.30 V vs. RHE for 15 min until a stable current was reached (Fig. 3**a**). Then, linear sweep voltammetry (LSV) curves were measured (Fig. 3**b-d**). The three samples displayed a clear increase of the current density in the presence of CO_2 compared to values obtained in an Ar-saturated electrolyte. Besides, the total current densities significantly increased with the loading of Poly-TAA-Co on CNTs (Fig. 4**a and** Figure S8**a**), indicating a faster reaction rate in the presence of pre-oxidized CNTs.

The Faradaic efficiency (FE) for CO_2 conversion to CO (FE_{CO}) and H_2 (FE_{H2}), and the related current density were determined in the potential range from −0.40 to −0.70 V vs. RHE. Fig. 4**b and** Figure S8**b** shows the FE_{CO} on these of the Poly-TAA-Co-based cathodes. The FE of bare CNTs can also be found in Fig. 4**b**. For Poly-TAA-Co-CNT(3:7) samples, the CO_2RR to CO started at a potential as low as −0.40 V vs. RHE with a maximum FE_{CO} of 90 % at −0.50 V vs. RHE. This FE_{CO} is clearly above those obtained from Poly-TAA-Co-CNT(1:1), Poly-TAA-Co and CNT

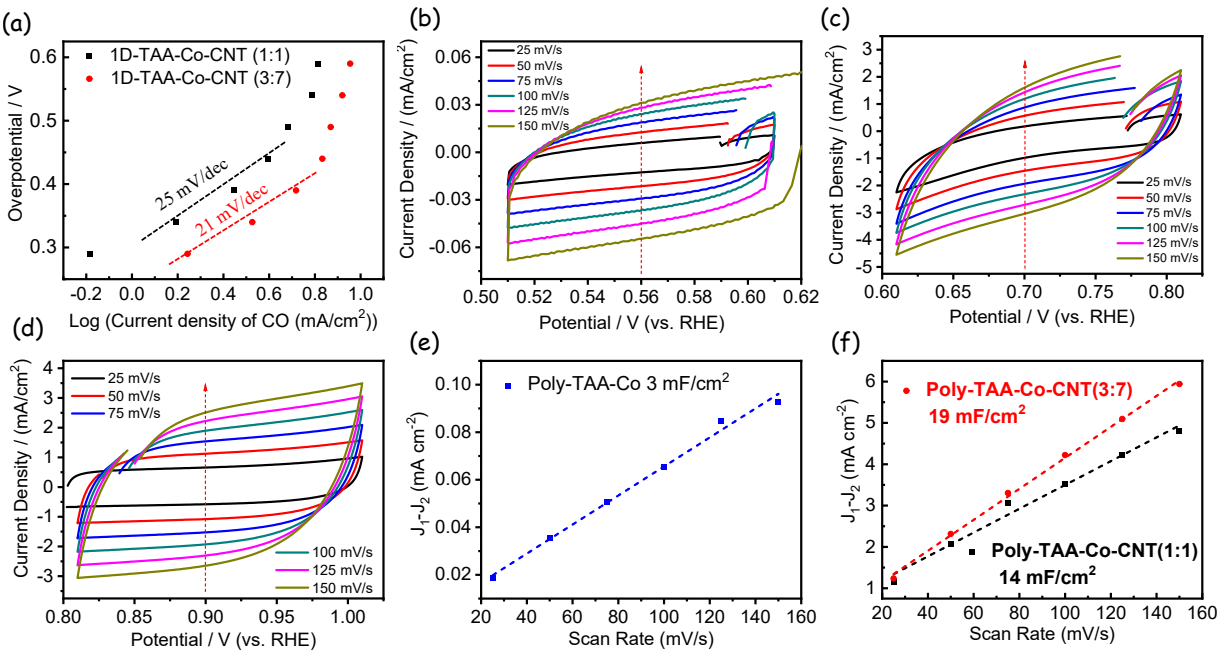

Fig. 5. (a) Tafel plots of Poly-TAA-Co-CNT (1:1), Poly-TAA-Co-CNT (3:7). Cyclic voltammograms curves for (b) Poly-TAA-Co, (c) Poly-TAA-Co-CNT(1:1) and (d) Poly-TAA-Co-CNT(3:7). Plots of the current density vs. scan rate for (e) Poly-TAA-Co, (f) Poly-TAA-Co-CNT(1:1) and Poly-TAA-Co-CNT(3:7) electrodes.

samples. Poly-TAA-Co-CNT(3:7) exhibits the highest current densities for CO formation among all the studied electrodes and in the whole range of applied potentials, with a maximum partial current density of -5.8 mA cm^{-2} at -0.50 V vs. RHE (Fig. 4**c**). It is attributed to higher conductivity with higher ratio of CNTs. As the potential changed to more negative values (from -0.55 to -0.70 V vs. RHE), the FE_{CO} of Poly-TAA-Co-CNT(1:1) and Poly-TAA-Co-CNT(3:7) gradually decreased and the competitive HER became the dominant reaction, as evidenced in the FE_{H2} and the partial H_2 current densities shown in Fig. 4**d** and **Figure S9**, respectively. Tafel plots were obtained by calculating the logarithm of current density [log(jCO)] vs. the overpotential (η) to reveal the possible reaction pathway of electrochemical CO_2 reduction

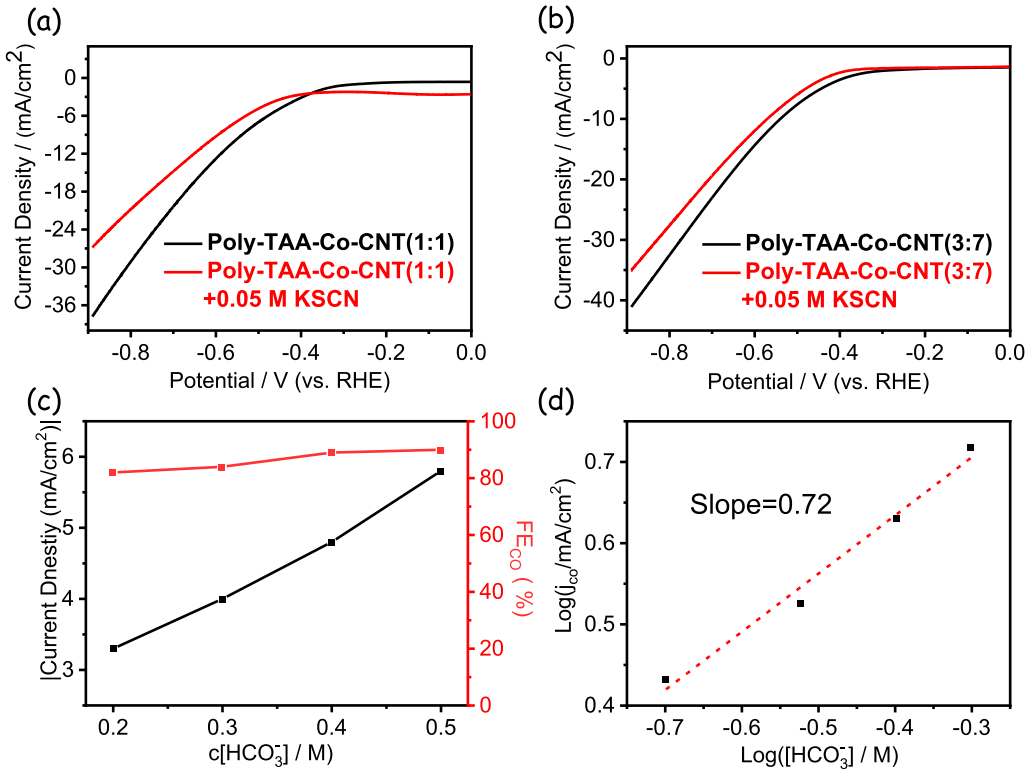

Fig. 6. (a) Poly-TAA-Co-CNT(1:1) and (b) Poly-TAA-Co-CNT(3:7) with and without 0.05 M KSCN. (c) Current density and FE of Poly-TAA-Co-CNT(3:7) at different KHCO3 concentrations at a constant potential (−0.50 V vs. RHE). (d) Partial CO current density of Poly-TAA-Co-CNT(3:7) vs. KHCO3 concentration at −0.50 V vs. RHE.

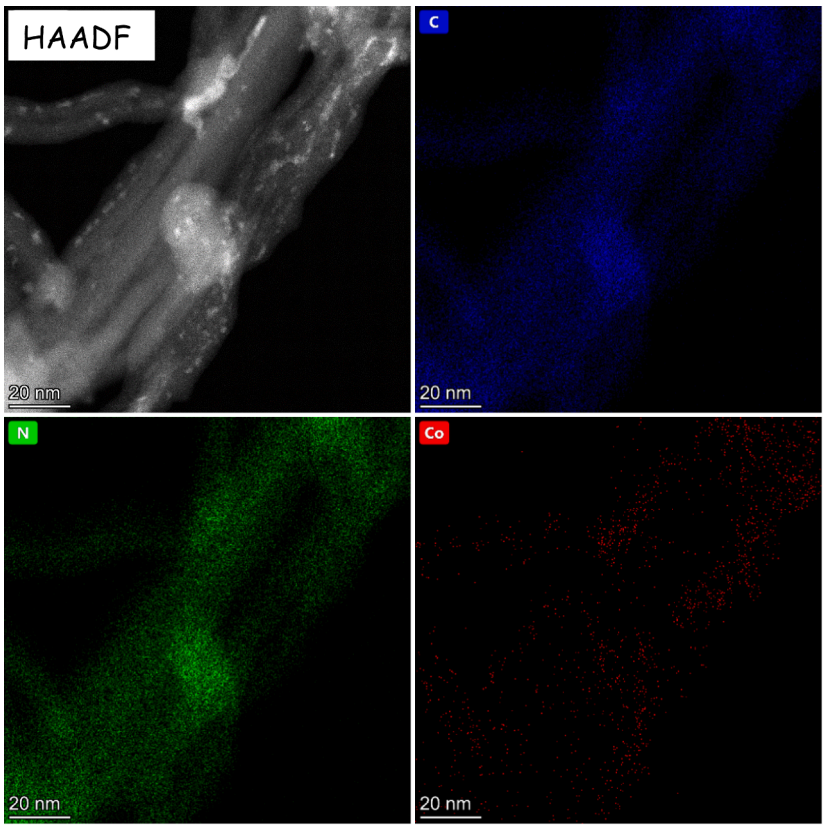

Fig. 7. EDX mapping of Poly-TAA-Co-CNT (3:7) after electrocatalytic CO_2RR.

(Fig. 5**a**). We obtained the plot in the linear part of low overpotentials ranging from −0.3 to −0.43 V and −0.28 to −0.38 V for Poly-TAA-Co-CNT(1:1) and Poly-TAA-Co-CNT(3:7), respectively. The Tafel slopes were calculated to be 25 mV dec^{-1} and 21 mV dec^{-1} for Poly-TAA-Co-CNT(1:1) and Poly-TAA-Co-CNT(3:7), respectively, indicating that the possible rate-determining step is a single electron transfer to CO_2 to generate a $CO_2^{\bullet-}$ intermediate, which is consistent with the previous report [16,33]. The EIS spectrum in **Figure S10** also confirmed a faster electron transfer when the Poly-TAA-Co was loaded on the surface of CNTs [23–26].

The electrochemical active surface area (ECSA) was determined from the electrochemical double-layer capacitance (C_{dl}) of the active materials (**see supporting information for details**). The C_{dl} of Poly-TAA-Co, Poly-TAA-Co-CNT(1:1) and Poly-TAA-Co-CNT (3:7) samples were obtained by CV at different scan rates, from the slope of $\Delta J = J_a - J_c$ against the scan rate (Fig. 5**b-d**), the slope which is twice of C_{dl} could be obtained. The C_{dl} of Poly-TAA-Co-CNT(1:1) and Poly-TAA-Co-CNT(3:7) samples are 14 mF cm^{-2} and 19 mF cm^{-2}, respectively, which are significantly larger values than the 3 mF cm^{-2} obtained from Poly-TAA-Co (Fig. 5**e-f**). Such different C_{dl} and thus of the related ECSA is a further indication of the higher CO_2RR catalytic activity of Poly-TAA-Co-CNT samples, and particularly of Poly-TAA-Co-CNT (3:7). In addition, the surface roughness factor (R_f) is calculated by taking the estimated ECSA and dividing by the geometric area of the electrode (1 cm^2). Generally, a constant capacitance is used in the same solution, therefore, R_f is linear with C_{dl}. The higher R_f obtained on the Poly-TAA-Co-CNT samples could significantly reduce the adhesion force between the electrode surface and gas bubbles, favoring the CO_2RR [25].

To further demonstrate the key role of tetra[14]anulene cobalt complex in the CO_2RR, we tested the catalytic activity of the samples after inactivating these sites by adding SCN^- ions which is with high affinity to Co into the solution. As shown in **Figure S11 and** Fig. 6**a-b**, upon addition of 0.05 M KSCN, a significant depression of the catalytic activity of Poly-TAA-Co, Poly-TAA-Co-CNT(1:1) and Poly-TAA-Co-CNT (3:7) was observed. This phenomenon is attributed to the poisoning of tetra[14]anulene cobalt active sites by SCN^-.

The current density at different HCO_3^- concentrations was measured at a constant applied potential of −0.50 V vs. RHE to probe the role of HCO_3^- within the reaction. As revealed in **Figure 6c-d, a** plot of log (j_{CO}) versus log ([HCO_3^-]) showed a slope of 0.72, suggesting that the concentration of HCO_3^- plays a considerable role, influencing the efficiency of the conversion reaction of CO_2 to CO. As observed previously that the HCO_3^- not only acts as a pH buffer and proton donor, but also increases the concentration of CO_2 near the electrode surface [25,27,28].

The CO_2RR performance of Poly-TAA-Co-CNT(3:7) was also compared with that of commercial cobalt phthalocyanine (CoPc) supported on CNTs (CoPc-CNT) at the same weight ratio (3:7) and with catalysts based non-polymerized Co-TAA molecules supported on CNTs (Co-TAA-CNT(3:7)). As shown in Fig. 4**e and Figure S12**, the maximum FE_{CO} obtained from Poly-TAA-Co-CNT(3:7) was significantly higher than those obtained from CoPc-CNT(3:7) and Co-TAA-CNT(3:7). These results demonstrated the higher activity of the Tetra[14]anulene cobat active site in Poly-TAA-Co-CNT, and also the important role of the conjugated polymer structure, which was proposed to favor the charge transfer during CO_2RR compared with non-polymeric Co-TAA.

The stability of the Poly-TAA-Co-CNT(3:7) electrocatalyst was evaluated through a 10 h durability test at a constant −0.50 V vs. RHE cathode potential. Outlet gases were analyzed every 30 min by GC to determine the FE_{CO}. The current density of Poly-TAA-Co-CNT(3:7) maintained a steady value of approximately −5.8 mA cm^{-2} with no significant decay (Fig. 4**f**) during the 10 h test. Besides, the corresponding FE_{CO} just slightly decreased from 90 % to 83 % after the 10 h stability test. From the measurement of the XRD pattern of the electrocatalysts before and after the CO_2RR stability test, no additional diffraction peak was observed, indicating no cobalt aggregating under

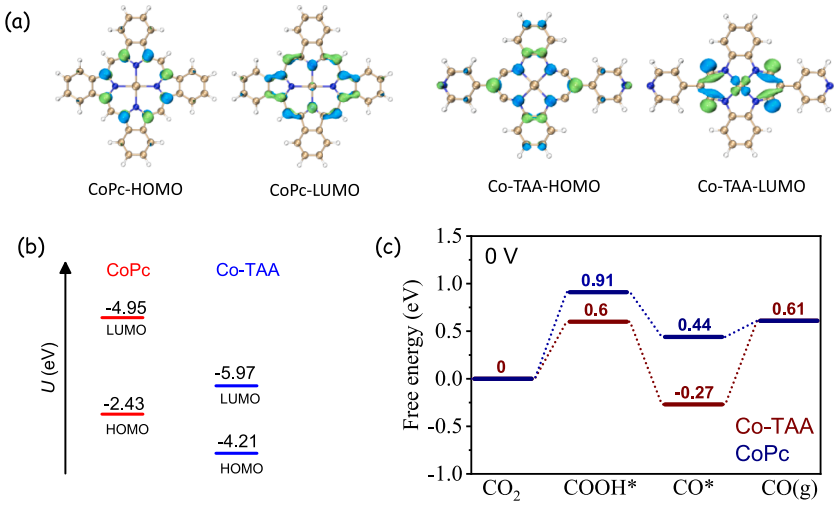

Fig. 8. DFT calculation results. (a). Calculated energy diagrams for CO_2 to CO conversion on CoPc and Co-TAA molecule, respectively. (b-c). Calculated electron density distribution of the highest occupied molecular orbital (HOMO) and lowest unoccupied molecular orbital (LUMO) levels of CoPc and Co-TAA.

CO_2RR conditions (Figure S13). The HAADF-STEM and HRTEM images (Figure S14) also confirm that no Co-based nanoparticles or clusters appear after the test and no significant change in the morphology of the studied catalysts. Furthermore, the EELS (Figure S15) and EDX (Fig. 7) elemental maps also confirm that the remaining Co atoms maintain a uniform dispersion. The inductively coupled plasma optical emission spectrometry (ICP-OES) was further used to analyzed the electrolyte during CO_2RR stability test, the Co signal was found, indicating that there is leaching of Co during the electrochemical CO_2RR process.

To further understand the high catalytic activity of the cobalt active site in Poly-TAA-Co for CO_2RR, DFT calculations were conducted. We particularly analyzed the Kohn-Sham molecular orbital of CoPc and the structure unit namely Co-TAA of Poly-TAA-Co (Fig. 8**a-b**). The energy of the lowest unoccupied molecular orbital (LUMO) of Co-TAA is −5.97 eV, which is below that of the CoPc molecule, −4.95 eV. The lower reduction potential of Co-TAA indicates that it is easier for Co-TAA to accept the charge transfer from the electrode to promote the CO_2RR.

The Gibbs free energy diagram of the CO_2RR for CoPc and Co-TAA are shown in Fig. 8**c**. The rate-determining step (RDS) for CO_2RR is the adsorption of CO_2 on the cobalt center to form *COOH by a proton-couple electron transfer reaction. At 0 V, the free energy of RDS for Co-TAA is 0.6 eV, which is lower than the 0.91 eV obtained for CoPc. Furthermore, under −0.5 V (Figure S16), the free energy of RDS for Co-TAA (0.1 eV) is still significantly lower than that of CoPc (0.41 eV). These DFT results are in good agreement with the experimental data.

4. Conclusions

We have reported for the first time a synthetic route to obtain new π-d conjugated cobalt building blocks based on Tetraaza[14]annulene organic polymer by a non-template method. Upon loading the cobalt-based macromolecule complex on the conductive carbon nanotube, the catalyst showed an excellent performance toward electrocatalytic CO_2 reduction, with a FE_{CO} of 90% at a low overpotential (390 mV) and a stable performance (>10 h). DFT simulations revealed the Co-TAA active sites to have the lowest activation energy for CO_2RR, well below that of commercial CoPc. Our results not only demonstrate that the non-template synthesis method can be used to synthesize tetra[14]annulene organic polymer, but also provide a new strategy to design tetra[14]annulene metal organic polymer based atomically dispersed metal atom catalyst for efficient CO_2RR and opens the way to use this type of materials for other applications.

Declaration of Competing Interest

The authors declare the following financial interests/personal relationships which may be considered as potential competing interests: Jordi Arbiol reports financial support was provided by Spanish MINECO. Jordi Arbiol reports financial support was provided by Government of Catalonia. Jordi Arbiol reports financial support was provided by Horizon 2020. Jordi Arbiol reports financial support was provided by MCIN. Jordi Llorca reports financial support was provided by European Regional Development Fund. Xiang Wang reports financial support was provided by China Scholarship Council. PengYi Tang reports financial support was provided by Humboldt Research Fellowship. Lijia Liu reports financial support was provided by Natural Sciences and Engineering Research Council Canada. Mohsen Shakouri reports financial support was provided by Canada Foundation for Innovation. Mohsen Shakouri reports financial support was provided by National Research Council. Mohsen Shakouri reports financial support was provided by Government of Saskatchewan. Weiqiang Tang reports financial support was provided by Chinese Postdoctoral Science Foundation.

Acknowledgements

The present work is supported by the projects SEHTOP, ENE2016-77798-C4-3-R, COMBENERGY (PID2019-105490RB-C32) and NANOGEN (PID2020-116093RB-C43), funded by MCIN/ AEI/10.13039/501100011033/ and by "ERDF A way of making Europe", by the "European Union". This study was supported by MCIN with funding from European Union NextGenerationEU (PRTR-C17.I1) and the Government of Catalonia. ICN2 is supported by the Severo Ochoa program from Spanish MINECO (Grant No. SEV-2017-0706) and ICN2 and IREC are funded by the CERCA Programme /Generalitat de Catalunya. Part of the present work has been performed in the of the Universitat Autònoma de Barcelona Materials Science PhD program. Z.F Liang acknowledges funding from MINECO SO-FPT PhD grant (SEV-2013-0295-17-1). X. Wang and T. Zhang thank the China Scholarship Council, China, for the scholarship support. W. Tang thanks China Postdoctoral Science Foundation (Nos.2021M691008). Authors acknowledge funding from Generalitat de Catalunya 2017SGR327 and 2017SGR1246. This research was supported by JSPS KAKENHI Grant Numbers JP20K15293 (TY). M. Yamashita thanks the support from the 111 project (B18030) from China. The X-ray absorption fine structure was collected on the BL-12C beamline in the Photon Factory of the High Energy Accelerator Research Organization (KEK, proposal no. 2019G117, 2021G129). We thank Dr.

Guillaume Sauthier and Dr. Albert Llorente Mola for the great help on XPS and BET measurements, respectively.

Appendix A. Supplementary data

Supplementary data to this article can be found online at https://doi.org/10.1016/j.cej.2022.136129.

References

[1] A.R. Cutler, D. Dolphin, A mechanistic study of metal template syntheses of dibenzo-tetraaza(14)annulene macrocyclic complexes, J. Coord. Chem. 6 (1) (1976) 59–61.

[2] C.W. Marvin, G. Guy, L.G. Virgil, Crystal and molecular structure of the macrocyclic nickel(II) complex [Ni($C_{18}H_{14}N_4$)]: dibenzo[b, i][1,4,8,11]tetraaza [14]annulenenickel(II), Inorg. Chem. 16 (1977) 305–310.

[3] M. Philip, Dibenzotetraaza[14]annulenes: versatile ligands for transition and main group metal chemistry, Chem. Soc. Rev. 27 (1998) 105–115.

[4] F.A. Cotton, J. Czuchajowska, Recent developments in the chemistry of mono- and dinuclear complexes of the macrocyclic dianion, 5,7,12,14-tetramethyldibenzo[b, i][1,4,8,11] tetraazac, Polyhedron 9 (21) (1990) 2553–2566.

[5] A.M. Whyte, Y. Shuku, G.S. Nichol, M.M. Matsushita, K. Awaga, N. Robertson, Planar Ni(ii), Cu(ii) and Co(ii) tetraaza[14]annulenes: structural, electronic and magnetic properties and application to field effect transistors, J. Mater. Chem. 22 (2012) 17967–17975.

[6] Z. Liang, M. Damjanović, M. Kamila, G. Cosquer, B.K. Breedlove, M. Enders, M. Yamashita, Proton control of the lanthanoid single-ion magnet behavior of a double-decker complex with an indolenine-substituted annulene ligand, Inorg. Chem. 56 (11) (2017) 6512–6521.

[7] A. Chirila, B. Gopal Das, N.D. Paul, B. de Bruin, Diastereoselective radical-type cyclopropanation of electron-deficient alkenes mediated by the highly active cobalt (II) tetramethyltetraaza[14]annulene catalyst, ChemCatChem 9 (8) (2017) 1413–1421.

[8] A.Q. Ramle, H. Khaledi, A.H. Hashim, M.A. Mingsukang, A.K. Mohd Arof, H.M. Ali, W.J. Basirun, Indolenine-dibenzotetraaza [14] annulene Ni (II) complexes as sensitizers for dye-sensitized solar cells, Dyes Pigm. 164 (2019) 112–118.

[9] Y. Jiang, I. Oh, S.H. Joo, O. Buyukcakir, X. Chen, S.H. Lee, M. Huang, W.K. Seong, S.K. Kwak, J.W. Yoo, R.S. Ruoff, J. Am. Chem. Soc. 141 (2019) 16884–16893.

[10] T. Zhang, X. Han, H. Liu, M. Biset-Peiró, X. Zhang, P. Tan, P. Tang, L. Zheng, B. Yang, J.R. Morante, J. Arbiol, Quasi-double-star nickel and iron active sites for high-efficient carbon dioxide electroreduction, Energy Environ. Sci. 14 (2021) 4847–4857.

[11] Z. Gu, H. Shen, Z. Chen, Y. Yang, C. Yang, Y. Ji, Y. Wang, C. Zhu, J. Liu, J. Li, T.-K. Sham, X. Xu, G. Zheng, Efficient electrocatalytic CO_2 reduction to C_{2+} alcohols at defect-site-rich Cu surface, Joule 5 (2) (2021) 429–440.

[12] Z.-Z. Wu, F.-Y. Gao, M.-R. Gao, Regulating the oxidation state of nanomaterials for electrocatalytic CO_2 reduction, Energy Environ. Sci. 14 (3) (2021) 1121–1139.

[13] S. Lin, C.S. Diercks, Y.B. Zhang, N. Kornienko, E.M. Nichols, Y. Zhao, A.R. Paris, D. Kim, P. Yang, O.M. Yaghi, C.J. Chang, Covalent organic s comprising cobalt porphyrins for catalytic CO_2 reduction in water, Science 11 (2015) 1208–1213.

[14] Y. Wu, Z. Jiang, X.u. Lu, Y. Liang, H. Wang, Domino electroreduction of CO_2 to methanol on a molecular catalyst, Nature 575 (7784) (2019) 639–642.

[15] Z. Liang, H.Y. Wang, H. Zheng, W. Zhang, R. Cao, Porphyrin-based s for oxygen electrocatalysis and catalytic reduction of carbon dioxide, Chem. Soc. Rev. 50 (2021) 2540–2581.

[16] N.a. Han, Y.u. Wang, L.u. Ma, J. Wen, J. Li, H. Zheng, K. Nie, X. Wang, F. Zhao, Y. Li, J. Fan, J. Zhong, T. Wu, D.J. Miller, J. Lu, S.-T. Lee, Y. Li, Supported cobalt polyphthalocyanine for high-performance electrocatalytic CO_2 reduction, Chem 3 (4) (2017) 652–664.

[17] X. Zhang, Y. Wang, M. Gu, M. Wang, Z. Zhang, W. Pan, Z. Jiang, H. Zheng, M. Lucero, H. Wang, G.E. Sterbinsky, Q. Ma, Y.-G. Wang, Z. Feng, J. Li, H. Dai, Y. Liang, Molecular engineering of dispersed nickel phthalocyanines on carbon nanotubes for selective CO_2 reduction, Nature Energy 5 (9) (2020) 684–692.

[18] X. Zhang, Z. Wu, X. Zhang, L. Li, Y. Li, H. Xu, X. Li, X. Yu, Z. Zhang, Y. Liang, H. Wang, Highly selective and active CO_2 reduction electrocatalysts based on cobalt phthalocyanine/carbon nanotube hybrid structures, Nat. Commun. 8 (2017) 14675.

[19] J. Su, J.-J. Zhang, J. Chen, Y. Song, L. Huang, M. Zhu, B.I. Yakobson, B.Z. Tang, R. Ye, Building a stable cationic molecule/electrode interface for highly efficient and durable CO_2 reduction at an industrially relevant current, Energy Environ. Sci. 14 (1) (2021) 483–492.

[20] M. Zhu, R. Ye, K. Jin, N. Lazouski, K. Manthiram, Elucidating the reactivity and mechanism of CO_2 electroreduction at highly dispersed cobalt phthalocyanine, ACS Energy Lett. 3 (6) (2018) 1381–1386.

[21] Z. Jiang, Y. Wang, X. Zhang, H. Zheng, X. Wang, Y. Liang, Revealing the hidden performance of metal phthalocyanines for CO_2 reduction electrocatalysis by hybridization with carbon nanotubes, Nano Res. 12 (9) (2019) 2330–2334.

[22] H. Khaledi, M.M. Olmstead, H. Mohd Ali, N.F. Thomas, Indolenine meso-substituted dibenzotetraaza[14]annulene and its coordination chemistry toward the transition metal ions Mn(III), Fe(III), Co(II), Ni(II), Cu(II), and Pd(II), Inorg. Chem. 52 (4) (2013) 1926–1941.

[23] O.S. Bushuyev, P. De Luna, C.T. Dinh, L. Tao, G. Saur, J. van de Lagemaat, S. O. Kelley, E.H. Sargent, What should we make with CO_2 and how can we make it? Joule 2 (5) (2018) 825–832.

[24] W. Ren, X. Tan, W. Yang, C. Jia, S. Xu, K. Wang, S.C. Smith, C. Zhao, Isolated diatomic Ni-Fe metal-nitrogen sites for synergistic electroreduction of CO_2, Angew. Chem. Int. Ed. 58 (21) (2019) 6972–6976.

[25] C. Zhao, Y.u. Wang, Z. Li, W. Chen, Q. Xu, D. He, D. Xi, Q. Zhang, T. Yuan, Y. Qu, J. Yang, F. Zhou, Z. Yang, X. Wang, J. Wang, J. Luo, Y. Li, H. Duan, Y. Wu, Y. Li, Solid-diffusion synthesis of single-atom catalysts directly from bulk metal for efficient CO_2 reduction, Joule 3 (2) (2019) 584–594.

[26] C.F. Wen, F. Mao, Y. Liu, X.Y. Zhang, H.Q. Fu, L.R. Zheng, P.F. Liu, H.G. Yang, Nitrogen-stabilized low-valent Ni motifs for efficient CO_2 electrocatalysis, ACS Catal. 10 (2) (2020) 1086–1093.

[27] J. Gu, C.-S. Hsu, L. Bai, H.M. Chen, X. Hu, Atomically dispersed Fe3+ sites catalyze efficient CO_2 electroreduction to CO, Science 364 (6445) (2019) 1091–1094.

[28] T. Li, C. Yang, J.-L. Luo, G. Zheng, electrolyte driven highly selective CO_2 electroreduction at low overpotentials, ACS Catal. 9 (11) (2019) 10440–10447.

[29] H.J. Zhu, M. Lu, Y.R. Wang, et al., Efficient electron transmission in covalent organic nanosheets for highly active electrocatalytic carbon dioxide reduction, Nat. Commun. 11 (2020) 497.

[30] Y. Hu, N. Goodeal, Y. Chen, A.M. Ganose, R.G. Palgrave, H. Bronstein, M.O. Blunt, Chem. Commun. 52 (2016) 9941.

[31] S.-I. Yamazaki, M. Asahi, Z. Siroma, T. Ioroi, Electrochemical CO oxidation by a Rh tetraaza[14]annulene-based catalyst, ChemCatChem 12 (10) (2020) 2717–2720.

[32] H. Yang, L. Shang, Q. Zhang, R. Shi, G.I. Waterhouse, L. Gu, T. Zhang, A universal ligand mediated method for large scale synthesis of transition metal single atom catalysts, Nat. Commun. 10 (2019) 4585.

[33] Y. Chen, C.W. Li, M.W. Kanan, Aqueous CO_2 reduction at very low overpotential on oxide-derived Au nanoparticles, J. Am. Chem. Soc. 134 (49) (2012) 19969–19972.

[34] X. Huang, P. Sheng, Z. Tu, F. Zhang, J. Wang, H. Geng, Y. Zou, C. Di, Y. Yi, Y. Sun, W. Xu, D. Zhu, A two-dimensional π–d conjugated coordination polymer with extremely high electrical conductivity and ambipolar transport behaviour, Nat. Commun. 6 (2015) 7408.

[35] Y. Chen, M.i. Tang, Y. Wu, X. Su, X. Li, S. Xu, S. Zhuo, J. Ma, D. Yuan, C. Wang, W. Hu, A one-dimensional π–d conjugated coordination polymer for sodium storage with catalytic activity in negishi coupling, Angew. Chem. Int. Ed. 131 (41) (2019) 14873–14881.

[36] L. Wang, Y. Ni, X. Hou, L.i. Chen, F. Li, J. Chen, A two-dimensional metal-organic polymer enabled by robust nickel-nitrogen and hydrogen bonds for exceptional sodium-ion storage, Angew. Chem. Int. Ed. 59 (49) (2020) 22126–22131.

[37] K. Fan, C. Zhang, Y. Chen, Y. Wu, C. Wang, The chemical states of conjugated coordination polymers, Chem 7 (5) (2021) 1224–1243.

[38] Y. Ni, L. Lin, Y. Shang, L. Luo, L. Wang, Y. Lu, Y. Li, Z. Yan, K. Zhang, F. Cheng, J. Chen, Regulating electrocatalytic oxygen reduction activity of a metal coordination polymer via d–π conjugation, Angew. Chem. Int. Ed. 60 (31) (2021) 16937–16941.

[39] J. Hao, H. Zhu, Y. Li, P. Liu, S. Lu, F. Duan, W. Dong, Y. Lu, T. Liu, M. Du, Tuning the electronic structure of AuNi homogeneous solid-solution alloy with positively charged Ni center for highly selective electrochemical CO_2 reduction, Chem. Eng. J. 404 (2021) 126523.

[40] R. Shi, J. Guo, X. Zhang, G.I.N. Waterhouse, Z. Han, Y. Zhao, L. Shang, C. Zhou, L. Jiang, T. Zhang, Efficient wettability-controlled electroreduction of CO_2 to CO at Au/C interfaces, Nat. Commun. 11 (2020) 3028.

[41] Y.-R. Wang, R.-X. Yang, Y. Chen, G.-K. Gao, Y.-J. Wang, S.-L. Li, Y.Q. Lan, Chloroplast-like porous bismuth-based core-shell structure for high energy efficiency CO_2 electroreduction, Sci. Bull. 65 (2020) 1635–1642.

[42] D. L. T. Nguyen, Y. Kim, Y. J. Hwang, D. H. Won, Progress in development of electrocatalyst for CO_2 conversion to selective CO production, Carbon Energy 2 (2020), 72-98.

[43] H. Yang, L. Shang, Q. Zhang, R. Shi, G.I. Waterhouse, L. Gu, T. Zhang, A universal ligand mediated method for largescale synthesis of transition metal single atomcatalysts, Nat. Commun. 10 (2019) 4585.

[44] Y. Yao, Y. Zhu, C. Pan, C. Wang, S. Hu, W. Xiao, X. Chi, Y. Fang, J. Yang, H. Deng, S. Xiao, J. Li, Z. Luo, Y. Guo, Interfacial sp C-O–Mo hybridization originated high-current density hydrogen evolution, J. Am. Chem. Soc. 143 (2021) 8720–8730.

[45] D. Kim, J. Resasco, Y.i. Yu, A.M. Asiri, P. Yang, Yang, P, Synergistic geometric and electronic effects for electrochemical reduction of carbon dioxide using gold-copper bimetallic nanoparticles, Nat. Commun. 5 (1) (2014).

[46] S. Gao, Y. Lin, X. Jiao, Y. Sun, Q. Luo, W. Zhang, D. Li, J. Yang, Y. Xie, Partially oxidized atomic cobalt layers for carbon dioxide electroreduction to liquid fuel, Nature 529 (2016) 68–71.

[47] T. Zheng, K. Jiang, N.a. Ta, Y. Hu, J. Zeng, J. Liu, H. Wang, Large-scale and highly selective CO_2 electrocatalytic reduction on nickel single-atom catalyst, Joule 3 (1) (2019) 265–278.

[48] J. Pei, T. Wang, R. Sui, X. Zhang, D. Zhou, F. Qin, X.u. Zhao, Q. Liu, W. Yan, J. Dong, L. Zheng, A. Li, J. Mao, W. Zhu, W. Chen, Z. Zhuang, N-Bridged Co-N-Ni: new bimetallic sites for promoting electrochemical CO_2 reduction, Energy Environ. Sci. 14 (5) (2021) 3019–3028.

[49] B. Ravel, M. Newville, ATHENA, ARTEMIS, HEPHAESTUS: data analysis for X-ray absorption spectroscopy using IFEFFIT, J. Synchrotron Rad. 12 (4) (2005) 537–541.

[50] M. Newville, IFEFFIT: interactive XAFS analysis and FEFF fitting, J. Synchrotron Rad. 8 (2001) 322–324.

[51] J.J. Rehr, J. Mustre de Leon, S.I. Zabinsky, R.C. Albers, Theoretical x-ray absorption fine structure standards, J. Am. Chem. Soc. 113 (14) (1991) 5135–5140.

[52] H. Hu, J.Z. Ou, X. Xu, Y. Lin, Y. Zhang, H. Zhao, D. Chen, M. He, Y. Huang, L. Deng, Graphene-assisted construction of electrocatalysts for carbon dioxide reduction, Chem. Eng. J. 425 (2021) 130587.
[53] W. Ye, X. Guo, T. Ma, A review on electrochemical synthesized copper-based catalysts for electrochemical reduction of CO_2 to C2+ products, Chem. Eng. J. 414 (2021) 128825.
[54] G. Kresse, J. Furthmüller, Efficiency of ab-initio total energy calculations for metals and semiconductors using a plane-wave basis set, Comput. Mater. Sci. 6 (1) (1996) 15–50.
[55] G. Kresse, J. Furthmüller, Efficient iterative schemes for ab initio total-energy calculations using a plane-wave basis set, Phys. Rev. B: Condens. Matter. 54 (16) (1996) 11169–11186.
[56] C. Adamo, V. Barone, Toward reliable density functional methods without adjustable parameters: The PBE0 model, J. Chem. Phys. 110 (13) (1999) 6158–6170.
[57] P.C. Hariharan, J.A. Pople, the influence of polarization functions on molecular orbital hydrogenation energies, Teor. Chim. Acta 28 (3) (1973) 213–222.
[58] M.S. Gordon, The isomers of silacyclopropane, Chem. Phys. Lett. 76 (1980) (1980) 163–168.
[59] R.C. Binning, L.A. Curtiss, Compact contracted basis sets for third-row atoms: Ga-Kr, J. Comput. Chem. 11 (10) (1990) 1206–1216.
[60] D. Andrae, U. Häußermann, M. Dolg, H. Stoll, H. Preuß, Energy-adjustedab initio pseudopotentials for the second and third row transition elements, Teor. Chim. Acta 77 (2) (1990) 123–141.
[61] S. Grimme, S. Ehrlich, L. Goerigk, Effect of the damping function in dispersion corrected density functional theory, J. Comput. Chem. 32 (7) (2011) 1456–1465.
[62] M. J. Frisch, et al. Gaussian 16 (Gaussian 2016).
[63] J. Gao, Q. Shen, R. Guan, J. Xue, X. Liu, H. Jia, Q. Li, Y. Wu, Oxygen vacancy self-doped black TiO_2 nanotube arrays by aluminothermic reduction for photocatalytic CO_2 reduction under visible light illumination, J. CO_2 Util. 35 (2020) 205–215.
[64] Q. Shen, J. Xue, Y. Li, G. Gao, Q.i. Li, X. Liu, H. Jia, B. Xu, Y. Wu, S.J. Dillon, Construction of CdSe polymorphic junctions with coherent interface for enhanced photoelectrocatalytic hydrogen generation, Appl. Catal. B Environ. 282 (2021) 119552.
[65] T. Lu, F. Chen, Multiwfn: A Multifunctional Wavefunction Analyzer, J. Comput. Chem. 33 (2012) 580–592, https://doi.org/10.1002/jcc.22885.
[66] W. Humphrey, A. Dalke, K. Schulten, VMD: Visual Molecular Dynamics, J. Mol. Graph. Model. 14 (1996) 33–38, https://doi.org/10.1016/0263-7855(96)00018-5.
[67] T. Zhang, X. Han, H. Liu, M. Biset-Peiró, J. Li, X. Zhang, P. Tang, B. Yang, L. Zheng, J.R. Morante, J. Arbiol, Site-Specific Axial Oxygen Coordinated FeN4 Active Sites for Highly Selective Electroreduction of Carbon Dioxide. Adv. Funct. Mater. (2022) https://doi.org/10.1002/adfm.202111446. In press.